

TIME-DOMAIN CHARACTERIZATION OF DIODE MOUNTING STRUCTURES

E. Tentzeris, N. Dib, L. Katehi
University of Michigan, Ann Arbor

J. Oswald and P. Siegel
JPL

Abstract

The application of the FDTD technique in the calculation of the S-parameters of specific diode mounting and waveguide probe structures is discussed in this paper. Comparative results are given and the FDTD technique is evaluated as an optimized CAD tool.

Introduction

The finite difference time domain method is used in the RF characterization of diode mounting and waveguide probe structures. A variety of excitation functions are considered and their effect on numerical convergence is studied. One of these functions, the Gabor function, offers a wavelet-like behavior. This function is localized both in time and frequency domain and its characteristics can be chosen such that its spectral content is centered around a desired frequency. As a first step, a number of simple geometries are analyzed and the FDTD results are compared to data derived through the integral equation and finite element methods for validation purposes. The same technique has been applied to waveguide-probe structures and the S-parameters as a function of frequency have been evaluated.

Theory

The FDTD method is formulated by discretizing Maxwell's curl equations

$$\mu \frac{\partial \vec{H}}{\partial t} = -\nabla \times \vec{E} \quad (1)$$

$$\epsilon \frac{\partial \vec{E}}{\partial t} = \nabla \times \vec{H} \quad (2)$$

over a finite volume and approximating the derivatives with centered difference approximations [1].

To obtain discrete approximations to the curl Maxwell's equations, the centered difference approximation is used on both the time and space first-order partial derivatives. For convenience, the six field locations are considered to be interleaved in space as shown in Fig.1, which is a drawing of the FDTD unit cell. The entire computational domain is obtained by stacking these rectangular cubes into a larger rectangular volume. The x, y and z dimensions of the unit cell are Δx , Δy and Δz , respectively. The advantages of this field arrangement are that centered differences are utilized in the calculation of each field component and that continuity of tangential field components is automatically satisfied. Because there are only six unique field components within the unit cell, the six field components touching the shaded upper eighth of the unit cell in Fig.1 are considered to be a unit node with subscript indices i, j and k corresponding to the node numbers in the \hat{x} , \hat{y} and \hat{z} directions. This notation implicitly assumes the 1/2 space indices and thus simplifies the notation, rendering the formulas directly implementable on the computer. The time steps are indicated with the superscript n.

Due to the use of centered differences in these approximations, the error is second order in both the space and time steps; i.e., if Δx , Δy , Δz and Δt are proportional to Δl , then the global error is $O(\Delta l^2)$. The maximum time step that may be used is limited by the stability criterion of the finite difference equations,

$$\Delta t \leq \frac{1}{v_{max}} \cdot \left(\frac{1}{\Delta x^2} + \frac{1}{\Delta y^2} + \frac{1}{\Delta z^2} \right)^{-1/2} \quad (3)$$

where v_{max} is the maximum velocity of light in the computational volume. Typically, v_{max} will be the velocity of light in free space unless the entire volume is filled with dielectric. These equations will allow the approximate solution of $\vec{E}(r,t)$ and $\vec{H}(r,t)$ in the volume of the computational domain ; however, special consideration is required for the conductors, the mesh boundaries and the excitation.

The electric conductors are assumed to be perfectly conducting with zero thickness and are treated by setting the electric field components that lie on the conductors to zero.

Due to the finite capabilities of the computers used to implement the finite-difference equations, the mesh must be limited in the x, y and z directions. The difference equations cannot be used to evaluate the field components tangential to the outer boundaries since they would require the values of field components outside of the mesh. The tangential electric field components must be specified in such a way that outgoing waves are not reflected using absorbing boundary conditions. For TEM structures (e.g. coaxial) the pulses will be normally incident to the mesh walls. This leads to a simple approximate continuous absorbing boundary condition, which is that the tangential fields on the outer boundaries will obey the one-dimensional wave equation in the direction normal to the mesh wall. For the \hat{y} normal wall the one-dimensional wave equation may be written in the following form:

$$\left(\frac{\partial}{\partial y} - \frac{1}{v} \cdot \frac{\partial}{\partial t} \right) E_{tan} = 0 \quad (4)$$

This equation is Mur's first approximate absorbing boundary condition [2] and it may be easily discretized using only field components on or just inside the mesh wall yielding an explicit finite difference equation

$$E_0^{n+1} = E_1^n + \frac{v\Delta t - \Delta y}{v\Delta t + \Delta y} \cdot (E_1^{n+1} - E_0^n) \quad (5)$$

where E_0 represents the tangential electric field components on the mesh wall and E_1 represents the tangential electric field components one node inside of the mesh wall. Similar expressions are immediately obtained for the other absorbing boundaries by using the corresponding normal directions for each wall. The normal incidence assumption is not valid for the fringing fields which are propagating tangential to the walls. For this reason for non-TEM structures, the superabsorbance boundary condition is used in conjunction with the Mur's first ABC. The superabsorbance is a 2nd order ABC which takes into consideration both electric and magnetic fields [3].

The finite difference equations are used with the above boundary conditions to simulate the propagation of a preselected excitation function on the simulated structure. The essential aspects of the time-domain algorithm are as follows:

Three different functions have been used as excitations: First choice was the Gaussian pulse

$$f_0(t) = e^{-((t-t_0)/(pw))^2} \quad (6)$$

This is the most widely used excitation function, since it has the same shape in both time and frequency domains. Nevertheless, it contains a very strong D.C. component, which can be a possible cause for oscillations and slow convergence in structures that do not propagate the low frequencies (e.g. waveguides).

One excitation function that does not contain D.C. component is the Gaussian pulse derivative

$$f_1(t) = \frac{t - t_0}{pw^2} \cdot e^{-((t-t_0)/(pw))^2} \quad (7)$$

This function presents a better concentration around a specific central frequency than the gaussian pulse, but is still characterized by a significant low-frequency content.

Our final choice was the Gabor function

$$f_2(t) = e^{-((t-t_0)/(pw))^2} \sin(wt) \quad (8)$$

where

$$\begin{aligned} pw &= 2 \cdot \frac{\sqrt{6}}{\pi(f_{max} - f_{min})} \\ t_0 &= 2pw \\ w &= \pi(f_{min} + f_{max}) \end{aligned}$$

It can be easily observed that by modifying appropriately the parameters pw and w , we can restrict the frequency spectrum of the above function in a specific region $[f_{min}, f_{max}]$ (wavelet-like behavior). As a result, we can avoid all problems associated with D.C. or low frequency components without losing the time-bounded behaviour of the excitation function.

The above points can be easily observed from the time and frequency domain plots for all three excitation choices, which are presented in Fig. 1a (Gaussian pulse), 1b (Gaussian pulse derivative) and 1c (Gabor function).

Numerical Results

Numerical results have been computed for three configurations, an iris geometry and two waveguide probes. The first two configurations were used for the validation of the FDTD technique.

a. Rectangular iris geometry

The actual dimensions of this geometry are shown in Fig. 2a. There is a p.e.c. at the one end of the waveguide and the Gaussian pulse excitation impinges on the other end. We have calculated the S_{11} parameter using the FDTD technique at a position close to the iris. Input impedance for this configuration may be calculated from the $S_{11}(\omega)$ by transforming the reference plane for the S_{11} calculation to the reference plane of the input impedance calculation, through the formula

$$Z_{in} = Z_o \frac{1 + S_{11}e^{j2kL}}{1 - S_{11}e^{j2kL}} \quad (9)$$

where k is the wavenumber in the waveguide, L is the distance between the two reference planes and Z_o is the dominant mode wave impedance of the waveguide. Results for the input admittance and S_{11} at a plane parallel to the pec and at a distance $2a$ from it are shown in Fig. 2a. These results are compared with results obtained using the lumped-element technique and the agreement is very good (Fig. 2b).

b. Waveguide Probe

The waveguide-probe configuration of Fig. 3a was analyzed using the FDTD technique. The two probes are embedded on a dielectric slab with $\epsilon_r = 3.8$. The one end of the waveguide is short-circuited and the Gaussian pulse excitation is applied at the other end. We calculated the input impedance Z_{in} between the two probes, by using the relationship

$$Z_{in} = \frac{V}{I} \quad (10)$$

$$V = \oint \vec{E} \cdot \vec{dl} \quad (11)$$

$$I = \int \vec{H} \cdot \vec{dl} \quad (12)$$

The voltage V was calculated by integrating along a vertical path connecting the two probes and the current I by integrating along a horizontal closed loop at the plane located in the

middle of the distance between the two probes. Though V was independent on the choice of the paths, I was slightly sensitive to the closed-loop size. This sensitivity lessened as the dielectric was thinner, since it was due to the displacement current inside the dielectric. The results for the real part of the input impedance are compared with those obtained from Moment method technique and the agreement is again very good.(Fig. 3b)

c. Coaxial-fed probe

The geometry of Fig. 4a is similar to the geometry of the probe discussed above. Again, we had two probes embedded on a dielectric slab inside a waveguide. One end of the waveguide was short-circuited and we calculated the input impedance between the two probes. Nevertheless, there is a major difference between (B) and (C). Now the probes are coaxial (center) fed, however in (B) the excitation was applied at the input of the waveguide. That means that in (C) we have a near-field excitation, though in (B) we had a far-field.

As a first step of our simulation, the excitation pulse was impressed in the region between the two probes and we tried to calculate the input impedance by use of the formulas (10) - (12). This effort was unsuccessful, since the value of the current I became very sensitive on the size of the horizontal closed loop. This was due mainly to two factors, the displacement current and the fact that the edge conditions could not be perfectly satisfied.

To avoid the above problems the whole structure with the coaxial feed was analyzed. The feed was simulated with a rectangular 50Ω coaxial with $\epsilon_r=2.2$. The excitation pulse was applied at the input of the feed-line. In this way the problems coming from the near-field excitation vanished and the input impedance was calculated by use of the formula

$$Z_{in} = Z_o \frac{1 + S_{11}}{1 - S_{11}} \quad (13)$$

The results for the S_{11} are presented in Fig.4b . There is total reflection below the waveguide dominant mode cutoff frequency (2.89GHz). Above this frequency, propagation inside the waveguide magnifies and S_{11} starts decreasing.

We have to emphasize on the fact that around resonance, the calculation of Z_{in} from S_{11} by use of the above formula is characterized by very high numerical errors. For example, 1% error in S_{11} (0.993 instead of 0.983) due to computer round-off errors causes 145% error in Z_{in} (14236 instead of 5832 Ohm). As a result, the values of Z_{in} around resonance have no significant practical meaning.

Autoregressive predictors have been used to extrapolate accurately the calculated field values. As a result, the execution time has been reduced drastically by one order.

Conclusion

The finite-difference time-domain method has been used to perform time-domain simulations of pulse propagation in several waveguide probe and diode mounting structures. The frequency-dependent scattering parameters and the input impedance have been calculated by a Fourier transform of the time-domain results. These results have been verified successfully by comparison with other numerical techniques and with measured data. The versatility of

the FDTD method allows easy calculation for complicated structures. As the computational power of computers is rapidly increasing, this technique is very promising for the CAD of many types of waveguide probe and diode mounting structures.

Acknowledgement

This work was supported by the NASA Center for Space and Terahertz technology, University of Michigan, Ann Arbor.

References

- [1] K. S. Yee, "Numerical solution of initial boundary value problems involving Maxwell's equations in isotropic media," *IEEE Trans. Antennas Propagation*, pp. 302-307, May 1966.
- [2] G. Mur, "Absorbing boundary conditions for the finite-difference approximation of the time-domain electromagnetic-field equations," *IEEE Trans. Electromagnetic Compatibility*, pp. 377-382, Nov. 1981.
- [3] K. Mei and J. Fang, "Superabsorption-A method to improve absorbing boundary conditions," *IEEE Trans. Antennas Propagation*, pp. 1001-1010, Sep. 1992.

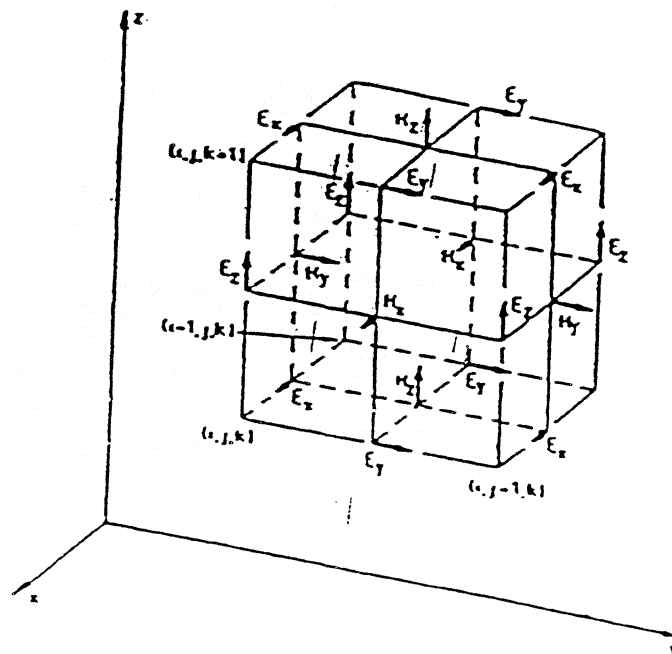


Fig. 1

$pw=0.1nsec, to=0.3nsec$

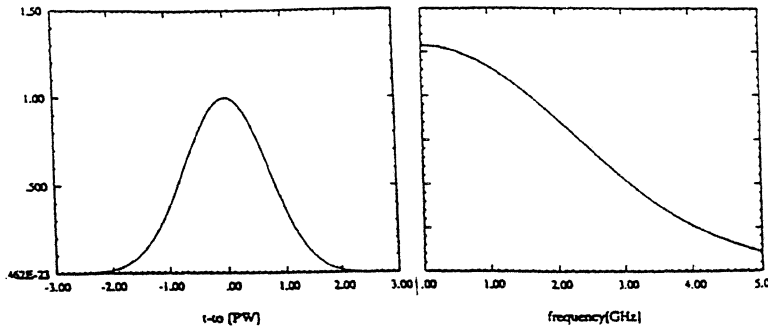


Fig. 1a

$pw=0.1nsec, to=0.3nsec$

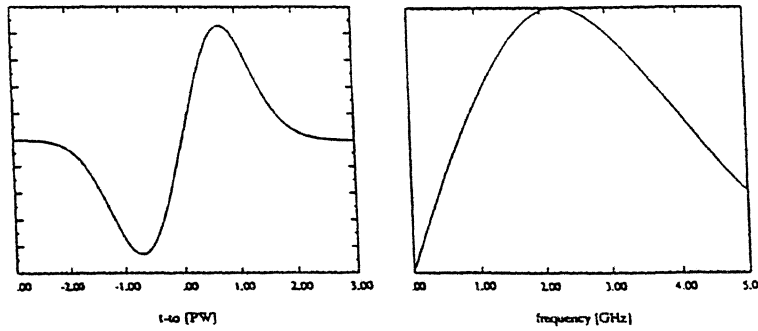


Fig. 1b

$pw=0.52nsec, to=1.04nsec$

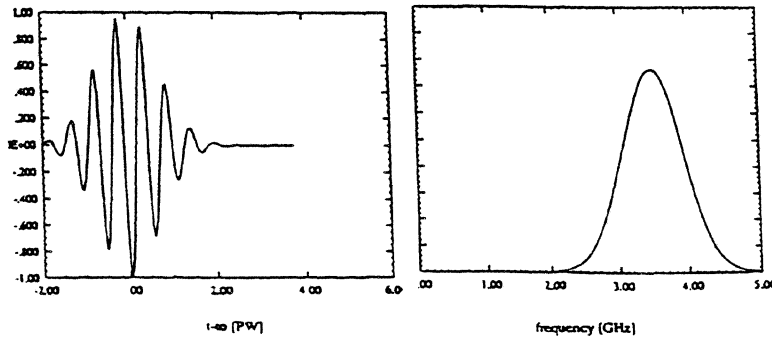


Fig. 1c

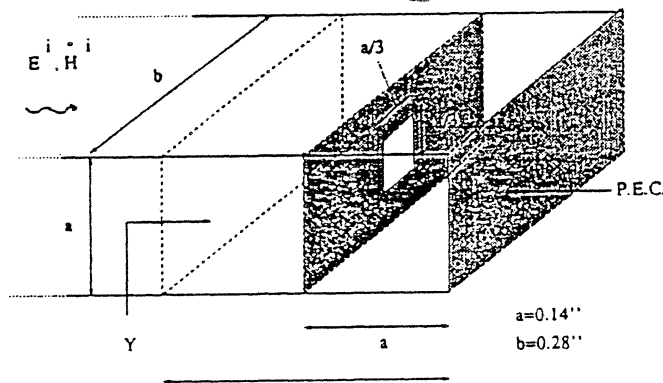


Fig. 2a

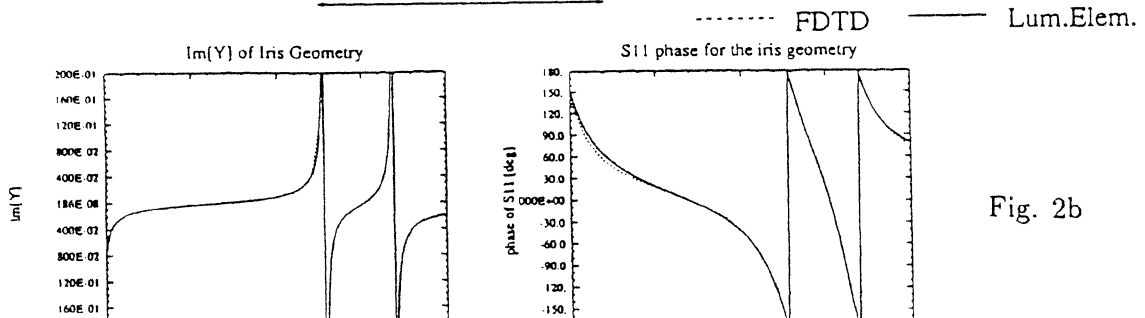


Fig. 2b

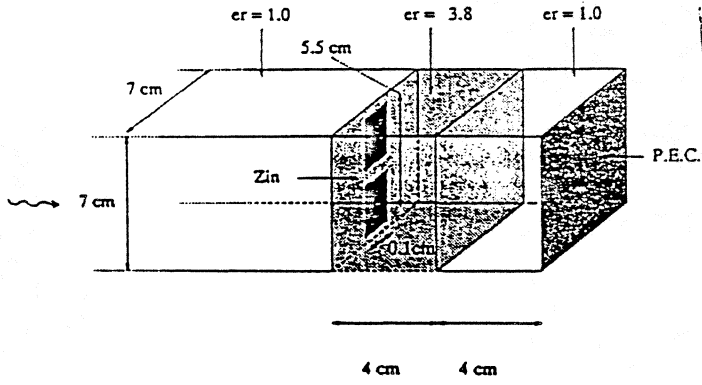


Fig. 3a

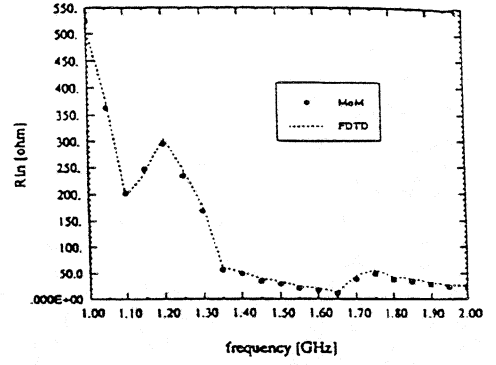


Fig. 3b

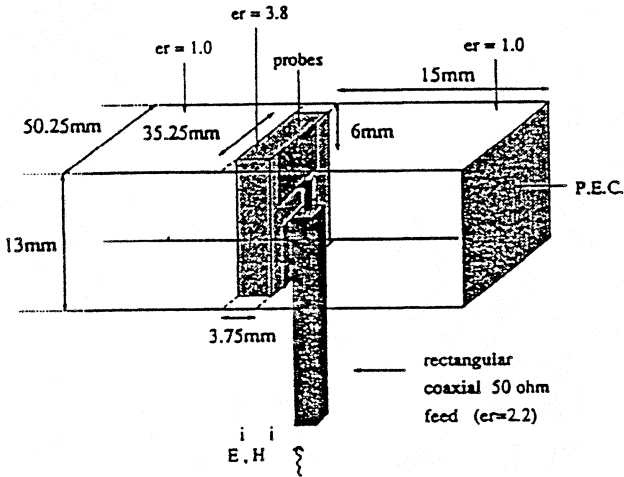


Fig. 4a

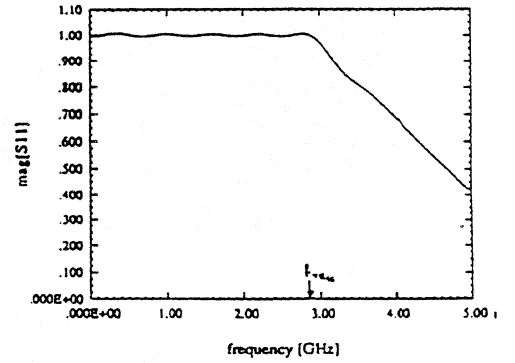


Fig. 4b